Fig. 4. Relative variation of the program window during cycling measured using a dc bias (solid line) and the pulsed tunnel technique (symbols) with three different waveforms.

decreased, thus shortening t_{PR}. In Fig. 3 t_{PR} is drawn against V_{CG} for the same value of ΔV_T (0.3 V, in this case). The main result was that t_{PR} dramatically decreases with the voltage and increasing V_{CG} respect to the dc case by a factor 1.3 (from 7 to 9.5 V) brings a reduction of t_{PR} by a factor 66 (from 10 ms to 150 μs).

Therefore, the goal of a fast FN tunnel programming has been achieved, with a slight increase of the program voltage which does not degrade data retention (as far as data retention can be correlated to SILC) and endurance: this can be seen in Fig. 4, where the relative variation of ΔV_T respect to the initial value ΔV_{T0} is plotted during cycling in several different conditions. In that experiment, the measure error was approximately 5%, which explains why we have a few data greater than unity.

In all the experiments erase was performed in the same dc conditions ($V_{CG} = -7$ V, $t_{PR} = 10$ ms) in order to ensure that the resulting variation were only due to the different programming conditions. As one can see, the two experienced conditions with 9.5 and 7.8 V reduce t_{PR} but do not degrade reliability respect to the dc case. On the contrary, the waveform with $V_{CG} = 11.5$ V causes a progressive window closure during cycling, probably because of a strong degradation of the nanocrystals interface where charge is definitely trapped [9]. Comparison between the dc and pulsed curves at the same V_{CG} (9.5 V) puts in evidence the improvement of reliability with the pulsed technique. The dc stress at $V_{CG} = 11.5$ V brought to the device a definitive break within 1000 cycles.

In conclusion, we demonstrated that pulsed FN tunnel programming of NC Flash memories ensures improvement of the program time with respect to dc tunnel programming without degrading reliability. In particular, a reduction of t_{PR} by a factor 66 (from 10 ms to 150 μs) is obtained by increasing V_{CG} only by a factor 1.3 (from 7 to 9.5 V).

REFERENCES

[1] B. De Salvo, G. Ghibaudo, G. Pananakakis, P. Masson, T. Baron, N. Buffet, A. Fernandes, and B. Guillaumot, "Experimental and theoretical investigation of nano-crystal and nitride-trap memory devices," *IEEE Trans. Electron Devices*, vol. 48, pp. 1789–94, Aug. 2001.

[2] S. Tiwari, F. Rana, H. I. Hanafi, A. Hartstein, E. Crabbe, and Chan, "A silicon nanocrystals-based memory," *Appl. Phys. Lett.*, vol. 69, no. 10, pp. 1377–80, 1996.

[3] C. Gerardi, G. Ammendola, M. Melanotte, S. Lombardo, and I. Crupi, "Reliability and retention study of nanocrystal cell arrays," in *Proc. ESS-DERC*, 2002, pp. 475–478.

[4] M. K. Cho and D. M. Kim, "High-performance SONOS memory cell free of drain turn-on and over-erase: Compatibility issue with current FLASH technology," *IEEE Electron Device Lett.*, vol. 21, pp. 399–402, Aug. 2000.

[5] F. Irrera and B. Riccò, "Pulsed tunnel programming of nonvolatile memories," *IEEE Trans. Electron Devices*, vol. 50, pp. 2474–2480, Dec. 2002.

[6] F. Irrera, "Degradation kinetics of thermal oxides," *Appl. Phys. Lett.*, vol. 79, pp. 182–184, 2001.

[7] F. Irrera and B. Riccò, "SILC dynamics in MOS structures subject to periodic stress," *IEEE Trans. Electron Devices*, vol. 49, pp. 1729–1735, Oct. 2003.

[8] J. H. Stathis, "Physical and predictive models of ultrathin oxide reliability in CMOS devices and circuits," *IEEE Trans. Device Mater. Rel.*, vol. 1, Dec. 2001.

[9] C. Monzio-Compagnoni *et al.*, "Study of nanocrystal memory reliability by CAST structures," in *Proc. IRPS*, 2003, p. 506.

Top-Emitting OLED Using Praseodymium Oxide Coated Platinum as Hole Injectors

Chengfeng Qiu, Huajun Peng, Haiying Chen, Zhiliang Xie, Man Wong, and Hoi Sing Kwok

Abstract—**Praseodymium oxide (Pr_2O_3) coated platinum (Pt) was investigated as a composite hole-injection layer for "top-emitting" organic light-emitting diodes (OLEDs) based on copper (II) phthalocyanine–N, N′-diphenyl-N, N′ bis(3-methylphenyl-1, 1′-biphenyl-4, 4′-diamine–tris-8-hydroxyquinoline aluminum. Aluminum was used as the current-carrying and reflecting anode electrode underneath the composite hole-injection layer. The resulting radiation pattern was found to be highly non-Lambertian. With 1-nm Pr_2O_3 on 2-nm Pt, a luminance of ~ 1400 cd/m^2 in the normal direction was obtained. When the intensity was integrated over all angles, it was determined that these OLEDs emitted 30% more radiation than their conventional "bottom-emitting" counterparts. An external quantum efficiency of 1.32% and a power efficiency of 1.1 lm/W were obtained at 100 cd/m^2. The difference between top- and bottom-emitting diodes is explained in terms of microcavity effects.**

Index Terms—**Microcavity effects, platinum, praseodymium oxide, top-emitting organic light-emitting diodes.**

I. INTRODUCTION

Organic light-emitting diodes (OLEDs) [1] are challenging liquid-crystals as an alternative flat-panel display technology because of their all solid-state nature, ease of manufacturing, faster switching speed and being self-emitting with a wider viewing angle.

Both passive- and active-matrix [2]–[4] displays based on OLEDs have been demonstrated. While the former are limited to simple area-

or small matrix-addressed displays, the latter are more applicable to higher information content applications. As the resolution is enhanced for a given size of a conventional through-the-glass "bottom-emitting" display, the fraction of the pixel area transparent to OLED emission is reduced. Consequently, a higher drive current is required to achieve a given pixel brightness. High current is undesirable because of the resulting higher power dissipation and reduced device lifetime [5].

The problem of diminishing aperture ratio is eliminated if a "top-emitting" pixel architecture is used [6]. All electronic devices are buried under an OLED that practically emits over the entire pixel area. In fact, a top-emitting architecture is required if the display is built on an opaque substrate, such as silicon. Besides the advantages of lower power dissipation and longer device lifetime resulting from a lower drive current, light coupling efficiency may also be enhanced due to the elimination of waveguide loss in the glass transmission medium.

Most of the reported top-emitting OLED structures employed the same organic/inorganic interfaces as the bottom-emitting ones, using semi-transparent films, such as MgAg [7] or LiF–Al [8]–[11] as cathodes, and conventional indium-tin oxide (ITO) on reflecting metals, such as ITO–Ag [10] or ITO–Al [9], [11], as anodes. However, the use of ITO as anodes demands a nontrivial patterning process and introduces a thickness-dependent spectral shift. Dobbertin *et al.* also reported an "inverted" structure with a sputtered top ITO *anode* [12], but the reported electrical performance was poorer than that of conventional bottom-emitting diodes, resulting in lower power efficiency.

In the present report, the fabrication and characterization of top-emitting OLEDs with composite anodes constructed of aluminum (Al)–platinum (Pt)–praseodymium oxide (Pr_2O_3) are described. Al was used as both a reflecting mirror and a low-resistance current-carrying interconnect. Pt provided the high work-function for more efficient hole injection. Since Pt had been shown to degrade emission efficiency [13], [14], a thin insulating Pr_2O_3 layer was added to enhance hole injection efficiency, while still maintaining a high emission efficiency [15].

The functional organic layers are copper (II) phthalocyanine (CuPc) as an anode buffer layer, N, N′-diphenyl-N, N′ bis(3-methylphenyl-1, 1′-biphenyl-4, 4′-diamine (TPD) as a hole-transport layer and tris-8-hydroxyquinoline aluminum (Alq_3) as an electron-transport and emission layer. Transparent cathodes were constructed of lithium fluoride (1 nm)–Al (12 nm)–ITO (50 nm). Top-emitting OLEDs constructed using the composite anodes were found to be more efficient than conventional bottom-emitting OLEDs. The observed improvement is explained in terms of microcavity effects.

II. OLED FABRICATION

The starting substrates were Al (100–nm) or ITO (75–nm) coated glass. The sequence of precleaning prior to loading into the evaporation chamber consisted of ultrasonic de-ionized (DI) water soak for 30 min, oven bake-dry for 1–2 h and ultraviolet/ozone (UV/O_3) treatment for 9 min [16].

Thin films of Pt (2 nm) and Pr_2O_3 (1 nm) were sequentially evaporated using 99.99% pure Pt wire and Pr_2O_3 powder loaded in resistively heated evaporation cells. The deposition rate was 0.01–0.03 nm/s. After the evaporation, the samples were subjected again to DI water rinse and UV/O_3 treatment. The constituent organic layers were next deposited using thermal vacuum evaporation of commercially available powder of CuPc, TPD and Alq_3. The base pressure in the evaporator was ~ 8 μtorr. The deposition rates of the organic thin films were 0.2–0.4 nm/s. The cathode consisted of sequential layers of 1 nm lithium fluoride (LiF), 12 nm semi-transparent Al and 50 nm dc-sputtered ITO [17]. The respective deposition rates of LiF,
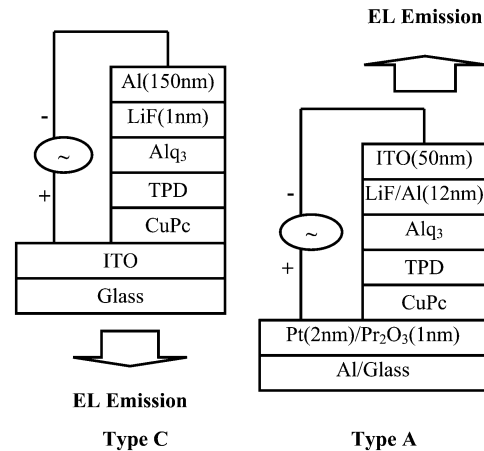

Fig. 1. Structural schematics of top-emitting (type A) and conventional bottom-emitting (type C) OLEDs.

Al, and ITO were 0.02–0.05, 1–1.5, and 0.05 nm/s. Film thicknesses were determined *in situ* using a crystal monitor.

Two types of OLEDs were fabricated for comparison:

Type A: Glass–Al(100 nm)–Pt(2 nm)–Pr_2O_3(1 nm)–CuPc–TPD–Alq_3–LiF–Al(12 nm)–ITO.
Type C: Glass–ITO(75 nm)–CuPc(20 nm)–TPD (40 nm)–Alq_3 (50 nm)–LiF(1 nm)–Al(150 nm).

Unless otherwise specified, the thickness values of the various films in a top-emitting type A diode are the same as those of the corresponding films in a conventional bottom-emitting type C diode. The structures of the OLEDs are schematically shown in Fig. 1.

The diodes were characterized in room ambient and temperature without encapsulation. Electroluminescent (EL) intensity was measured using a PR650 SpectraScan spectrophotometer. Current–voltage characteristics were measured using an Advantest R6145 dc voltage current source and Fluke 45 dual display multimeter. Top-emitting OLEDs without the Pt and Pr_2O_3 layers have also been fabricated. Because they were only weakly emitting, their characteristics will not be described in this report.

III. RESULTS AND DISCUSSION

The luminance (L)–current density $(J–V)$-voltage characteristics of types A and C diodes are shown in Fig. 2. It can be seen that V at a given J is almost the same for both types of diodes. Since LiF–Al composite layers were used as the active cathodes in both types of diodes (the ITO in type A diode serves simply as a current-carrying low resistance shunt), the low V for type A diodes is made possible by efficient hole injection by the Pt–Pr_2O_3 composite layers covering the Al anodes [13]–[15]. Unlike that of the significantly thicker patterned ITO anodes in conventional top-emitting OLEDs, the in-plane resistance of 2-nm Pt is too large to be measured. Consequently, it is not necessary to have the Pt layer patterned for pixel-to-pixel isolation.

At a given J, a lower L in the normal direction is measured for type A diodes when compared to type C reference diodes. The 5.5-V "optical" turn-on voltage, defined as the voltage required to generate an L of 1 cd/m^2, of type A diodes is higher than the 3.5 V of the type C reference diodes. A peak L of 1400 cd/m^2 in the normal direction has been obtained for type A diodes at a J of 920 A/m^2.

The emission spectra in the normal direction of types A and C diodes are compared in Fig. 3. It can be seen that the full width at half maximum of the spectrum of a type A diode is narrower than that of the
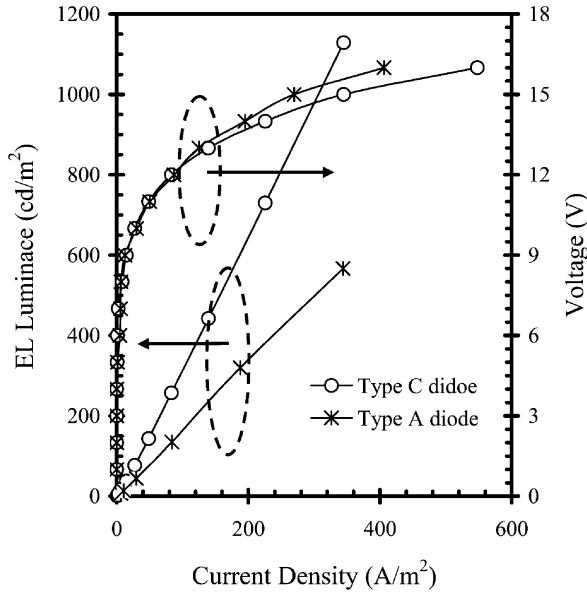
Fig. 2. EL luminance (L) in the normal direction; J–V characteristics of types A and C OLEDs.
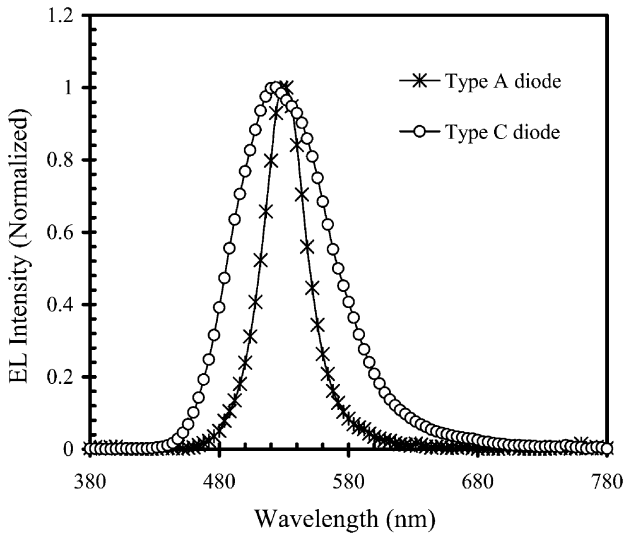

Fig. 3. EL spectra of types A and C OLEDs at normal direction.

conventional type C diode. For a type A diode, the reflectivity of the bottom anode mirror is $\sim 90\%$. The reflectivity of the semi-transparent cathode is $\sim 50\%$, much higher than the $\sim 5\%$ of the transparent ITO anode of a type C diode. While sensitive to the total thickness of the constituent organic layers, it is possible for these reflecting electrodes to yield a lower luminance in the normal direction of a type A diode, when compared to a conventional type C device with a highly transparent bottom anode.

Top-emitting OLEDs with reflecting anodes and cathodes are expected to exhibit strong microcavity effects on both the spectral and spatial distributions of the emission. A blue shift in the spectral peak with increasing angular displacement [9] from the normal has indeed been verified. The angular dependent luminance intensities of both top- and bottom-emitting OLEDs were measured, and normalized intensities were computed using the respective normal direction intensities as the bases. The corresponding angular distributions are compared in
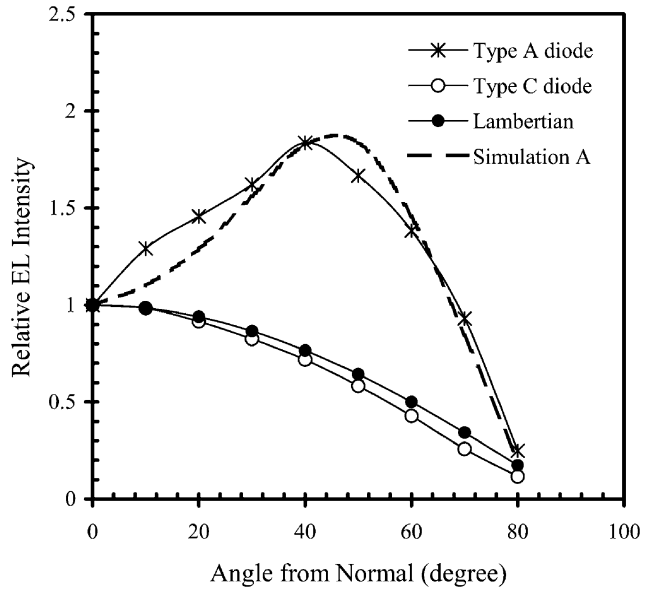

Fig. 4. Angular distribution of the EL intensity of the types A and C OLEDs.

Fig. 4. It is clear that while the angular dependence of the bottom-emitting OLED is well-fitted by a Lambertian distribution, the same is not true for the top-emitting OLED. In fact, the highest luminance was measured at $\sim 45°$ from the normal.

The strong microcavity effects in top-emitting OLEDs can also be quantified by calculating the spontaneous radiation of dipoles in thin-film microcavities [18]. The radiation mode is shown in the inset of Fig. 5. For a sheet of dipoles at a distance z from the bottom anode reflector (corresponding to reflectance r_1), the far-field emission intensity varies with the viewing angle θ as [18], [19]

$$I^{(s,p)}(\theta, \lambda) \propto \frac{\left| 1 + r_1^{(s,p)} \exp\left(\frac{j4\pi n_0 z \cos \theta_0}{\lambda} \right) \right|^2}{\left| 1 - r_1^{(s,p)} r_2^{(s,p)} \exp\left(\frac{j4\pi n_0 d \cos \theta_0}{\lambda} \right) \right|^2} \times T_2^{(s,p)}(\theta, \lambda) \quad (1)$$

where $r_2^{(s,p)}$ and T_2 are the respective reflectance and transmittance of the top semi-transparent cathode; s and p denote, respectively, the s and p polarization; n_0 is the refractive index of the medium between the electrodes; θ_0 is the internal emission angle that can be obtained using Snell's law; d is the effective cavity length; and λ is the emission wavelength in a vacuum. The numerator corresponds to the coupling between the cavity field and the dipole emission. The denominator is the cavity factor (also called the Airy factor) that represents interference effects in the cavity. The reflectance and transmittance at each interface were calculated using the transfer–matrix method [20]. The calculated radiation patterns for both the top- and bottom-emitting OLEDs are also shown in Fig. 4. Good agreement is obtained between the measured and the calculated radiation patterns.

In general, the external quantum efficiency (η_E) of an OLED can be evaluated by integrating the photon flux using the formula $2\pi \Sigma I(\theta) \sin(\theta) \Delta \theta$, where $I(\theta)$ is the measured photon radiation intensity at angle θ. The dependence of η_E on J for types A and C diodes is shown in Fig. 5. It is found that η_E of type A diodes is $\sim 1.3\%$ at a J of $190 \, \text{A/m}^2$. This is about 30% higher than that of the type C reference diodes. This result is consistent with previous discussion that top-emitting OLEDs could be more efficient than the corresponding bottom-emitting OLEDs [21]. Recently, Riel et $al.$ reported that by tuning the thickness of the capping layer, the outcoupled light inten-
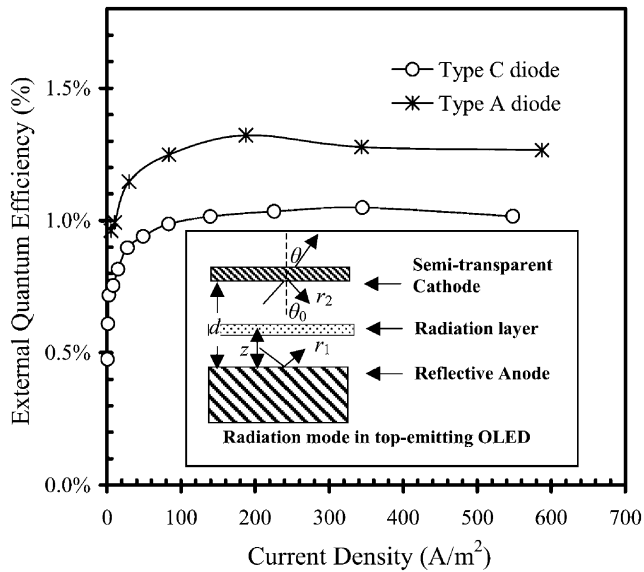
Fig. 5. External quantum efficiency $\eta_E - J$ characteristics of types A and C OLEDs.

sity could be enhanced by a factor of 1.7 [22]. Clearly, the efficiency of a top-emitting diode could be further enhanced with thickness optimization.

A power efficiency of 1.2 lm/W at a luminance of 100 cd/m^2 was measured for the top-emitting diodes. This is better than the recently published results [11], [12]. The better performance of the presently reported diodes is believed to result from the employment of the thin Pt–Pr$_2$O$_3$ hole injection layer. Reduction in operating voltage leads to lower power dissipation at equivalent luminance level.

IV. CONCLUSION

Through the use of Al as anode and thin platinum (Pt) and praseodymium oxide (Pr$_2$O$_3$) as hole injection layer, top-emitting OLEDs based on CuPc–TPD–Alq$_3$ have been investigated. It was found that this new top-OLED had strong microcavity effects. A luminance of 1400 cd/m^2 in the normal direction and an external quantum efficiency of 1.3% have been obtained in diodes with 2-nm Pt and 1-nm Pr$_2$O$_3$. Such diodes emitted 30% more photons than conventional bottom-emitting OLEDs, after integrating over all angles.

REFERENCES

[1] C. W. Tang and S. A. VanSlyke, "Organic electroluminescent diodes," *Appl. Phys. Lett.*, vol. 51, pp. 913–913, 1987.
[2] Z. Meng, H. Chen, C. Qiu, H. S. Kwok, and M. Wong, ""Active-matrix organic light-emitting diode display implemented using metal-induced unilaterally crystallized polycrystalline silicon thin-film transistors," in *SID Tech. Dig.*, 2001, pp. 380–383.
[3] Y. Shi, J. Bernkopf, S. Hermann, A. Hermanns, and D. Choquette, "Polymer light-emitting diode displays driven by integrated nanoblock ic drives," in *SID Tech. Dig.*, 2002, pp. 1092–1095.
[4] R. M. A. Dawason and M. G. Kane, "Pursuit of active matrix organic light emitting diode displays," in *SID Tech. Dig.*, 2001, pp. 372–375.

[5] S. A. Van Slyke, C. H. Chen, and C. W. Tang, "Organic electroluminescent devices with improved stability," *Appl. Phys. Lett.*, vol. 69, no. 15, pp. 2160–2160, 1996.
[6] G. W. Jones, "Active matrix OLED microdisplay," in *SID Tech. Dig.*, 2001, pp. 134–137.
[7] G. Gu, V. Bulovic, P. E. Burrows, S. R. Forrest, and M. E. Thompson, "Transparent organic light emitting devices," *Appl. Phys. Lett.*, vol. 68, pp. 2606–2606, 1996.
[8] L. S. Hung, C. W. Tang, M. G. Mason, P. Raychaudhuri, and J. Madathil, " High-efficiency top-emitting organic light-emitting devices," *Appl. Phys. Lett.*, vol. 78, pp. 544–544, 2001.
[9] F. Jean, J. Y. Mulot, B. Geffroy, C. Denis, and P. Cambon, "Microcavity organic light-emitting diodes on silicon," *Appl. Phys. Lett.*, vol. 81, pp. 1717–1717, 2002.
[10] M. H. Lu, M. S. Weaver, T. X. Zhou, M. Rothman, R. C. Kwong, M. Hack, and J. J. Brown, "High-efficiency top-emitting organic light-emitting devices," *Appl. Phys. Lett.*, vol. 81, pp. 3921–3921, 2002.
[11] S. Han, X. Feng, Z. H. Lu, D. Johnson, and R. Wood, "Transparent-cathode for top-emission light-emitting diodes," *Appl. Phys. Lett.*, vol. 82, pp. 2715–2715, 2003.
[12] T. Dobbertin, M. Kroeger, D. Heithecker, D. Schneider, D. Metzdorf, H. Neuner, E. Becker, H. H. Johannes, and W. Kowalsky, "Inverted top-emitting organic light-emitting diodes using sputter-deposited anodes," *Appl. Phys. Lett.*, vol. 82, pp. 284–284, 2003.
[13] C. Qiu, Z. Xie, H. Chen, M. Wong, and H. S. Kwok, "Comparative study of metal or oxide capped indium tin oxide anodes for organic light-emitting diodes," *J. Appl. Phys.*, vol. 93, pp. 3253–3253, 2003.
[14] Y. Shen, D. B. Jacobs, G. G. Malliaras, G. Koley, M. G. Spencer, and A. Ioannidis, "Modification of indium tin oxide for improved hole injection in organic light-emitting diodes," *Adv. Mater. Process.*, vol. 13, pp. 1234–1234, 2001.
[15] C. Qiu, H. Chen, Z. Xie, M. Wong, and H. S. Kwok, "Praseodymium oxide coated anode for organic light-emitting diodes," *Appl. Phys. Lett.*, vol. 80, pp. 3485–3485, 2002.
[16] C. Qiu, H. Chen, M. Wong, and H. S. Kwok, "Dependence of the current and power efficiencies of organic light-emitting diode on the thickness of the constituent organic layers," *IEEE Trans. Electron Devices*, vol. 48, pp. 2131–2131, Dec. 2001.
[17] H. Chen, C. Qiu, M. Wong, and H. S. Kwok, " DC sputtered indium-tin oxide transparent cathode for organic light-emitting diodes," *IEEE Electron Device Lett.*, vol. 24, pp. 315–315, Mar. 2003.
[18] H. Benisty, H. De Neve, and C. Weisbuch, "Impact of planar microcavity effects on light extraction-Part I: Basic concepts and analytical trends," *IEEE J. Quantum Electron.*, vol. 34, pp. 1612–1612, Dec. 1998.
[19] K. Neyts, P. de Visschere, D. K. Fork, and G. B. Anderson, "Semitransparent metal or distributed Bragg reflector for wide-viewing-angle LED microcavities," *J. Opt. Soc. Amer. B, Opt. Phys.*, vol. 17, pp. 114–114, 2000.
[20] M. Born and E. Wolf, *Principles of Optics*, Seventh ed.   Cambridge, U.K.: Cambridge Univ. Press, 1999.
[21] M. H. Lu and J. C. Sturm, "Optimization of external coupling and light emission in organic light-emitting devices: Modeling and experiment," *J. Appl. Phys.*, vol. 91, pp. 595–595, 2002.
[22] H. Riel, S. Karg, T. Beierlein, B. Ruhstaller, and W. Riess, "Phosphorescent top-emitting organic light-emitting devices with improved light outcoupling," *Appl. Phys. Lett.*, vol. 82, pp. 466–466, 2003.